

Simulations and Seasonal Prediction of the Asian Summer Monsoon in the NCEP Climate Forecast System

SONG YANG,* ZUQIANG ZHANG,⁺ VERNON E. KOUSKY,* R. WAYNE HIGGINS,* SOO-HYUN YOO,[#]
 JIANYIN LIANG,[@] AND YUN FAN[#]

*NOAA, Climate Prediction Center, Camp Springs, Maryland

⁺National Climate Center, China Meteorological Administration, Beijing, China

[#]RS Information System, Climate Prediction Center, Camp Springs, Maryland

[@]Institute of Tropical and Marine Meteorology, China Meteorological Administration, Guangzhou, China

(Manuscript received 19 March 2007, in final form 18 January 2008)

ABSTRACT

Analysis of the retrospective ensemble predictions (hindcasts) of the NCEP Climate Forecast System (CFS) indicates that the model successfully simulates many major features of the Asian summer monsoon including the climatology and interannual variability of major precipitation centers and atmospheric circulation systems. The model captures the onset of the monsoon better than the retreat of the monsoon, and it simulates the seasonal march of monsoon rainfall over Southeast Asia more realistically than that over South Asia. The CFS predicts the major dynamical monsoon indices and monsoon precipitation patterns several months in advance. It also depicts the interactive oceanic–atmospheric processes associated with the precipitation anomalies reasonably well at different time leads. Overall, the skill of monsoon prediction by the CFS mainly comes from the impact of El Niño–Southern Oscillation (ENSO).

The CFS produces weaker-than-observed large-scale monsoon circulation, due partially to the cold bias over the Asian continent. It tends to overemphasize the relationship between ENSO and the Asian monsoon, as well as the impact of ENSO on the Asian and Indo-Pacific climate. A higher-resolution version of the CFS (T126) captures the climatology and variability of the Asian monsoon more realistically than does the current resolution version (T62). The largest improvement occurs in the simulations of precipitation near the Tibetan Plateau and over the tropical Indian Ocean associated with the zonal dipole mode structure. The analysis suggests that NCEP's next operational model may perform better in simulating and predicting the monsoon climate over Asia and the Indo-Pacific Oceans.

1. Introduction

The Asian summer monsoon is characterized by the heaviest seasonal precipitation on earth and the most powerful heat source of the atmospheric circulation. It is an important climate system affecting the global climate and weather since fluctuations of the monsoon are often associated with floods, droughts, and other climate extreme events. Improvements in forecasting large monsoon anomalies can potentially lead to a reduction in loss of life and property in, and even outside, monsoon regions. Therefore, prediction of the monsoon has been a subject of long history (Blanford 1884;

Normand 1953) and is still an important subject in both the academic research community and operational forecasting groups (e.g., Webster et al. 1998; and see recent reviews in Wang 2006).

Numerical models have played a vital role in modern monsoon prediction. In particular, substantial efforts have been devoted to monsoon prediction by conducting experiments with individual models and by synthesizing work with multiple models and ensemble members (Sperber et al. 2001; Kang et al. 2002; Wang et al. 2004; Wu and Kirtman 2004; Annamalai et al. 2005). These efforts often involve evaluations of the performance of the models in simulating and predicting the monsoon. It is commonly believed that the overall skills of monsoon simulation and prediction increase when the quality of model features such as resolution, atmosphere–ocean–land coupling, and model physics is improved.

Corresponding author address: Dr. Zuqiang Zhang, CMA National Climate Center, 46 Zhongguancun Nandajie, Beijing 100081, China.
 E-mail: zhangzq@cma.gov.cn

The National Centers for Environmental Prediction (NCEP) Climate Forecast System (CFS) provides operational prediction of the world's climate including the Asian monsoon climate on different time scales. As described by Saha et al. (2006), the current CFS shows important advances in operational prediction from the previous dynamical forecast efforts by demonstrating a level of prediction skill comparable to statistical methods, at least for the United States. The CFS also demonstrates skills in simulating and predicting the variability of El Niño–Southern Oscillation (ENSO) (e.g., Wang et al. 2005), the climate over Africa (Thiaw and Mo 2005), and the subseasonal features of the Asian summer monsoon (Yang et al. 2008).

CFS products are now becoming an important source of information for regional climate prediction in many Asian countries where the monsoon climate dominates. For example, the CFS is one of the few coupled global operational models that participates in the annual forum on regional climate monitoring, assessment, and prediction for Asia, an activity encouraged by the World Meteorological Organization. However, at present, how competently the CFS performs in simulating and predicting the Asian monsoon climate remains unclear. Little is known about the model's ability in simulating the evolution of the monsoon and predicting the variability of the monsoon at different time leads.

In this study, we attempt to provide a comprehensive assessment of the ability of the CFS to simulate and predict the large-scale Asian monsoon, focusing on the climatology and interannual variability of the summer monsoon. We will show the strengths and weaknesses of the current operational forecast system in monsoon simulation, explain the model bias, reveal the dependence of prediction on lead time, and identify the source of skill for successful predictions. We will also show the possible improvement in monsoon simulation and prediction in a higher-resolution version of the CFS, which is considered the next version of the NCEP climate forecast model.

The rest of this paper is organized as follows: in section 2, we describe the basic features of the CFS, hindcast products of the model, and observational datasets that are used to verify the CFS output. In sections 3–5, we assess the performance of the CFS in simulating and predicting the Asian summer monsoon and demonstrate the degree of ENSO's effect on the skill of CFS in monsoon prediction. In section 6, we show the improvement in monsoon simulations by CFS as the resolution is increased from T62 to T126. A summary of the results obtained is provided in section 7.

2. Model, hindcast, and observational data

The NCEP CFS is a fully coupled dynamical prediction system (Saha et al. 2006). It has been an important component of the monthly to seasonal prediction system of the NCEP Climate Prediction Center (CPC) since it became operational in August 2004. The atmospheric component of CFS is the NCEP Global Forecast System model used for operational weather forecasting (Moorthi et al. 2001), except for a coarser horizontal resolution. It adopts a spectral triangular truncation of 62 waves (T62) in the horizontal and 64 sigma layers in the vertical with the top layer at 0.2 mb. The oceanic component of CFS is the NOAA Geophysical Fluid Dynamics Laboratory Modular Ocean Model V3.0 (Pacanowski and Griffies 1998). The model is global longitudinally and extends from 74°S to 64°N in latitude. The zonal resolution is 1°, and the meridional resolution is $\frac{1}{3}^\circ$ between 10°S and 10°N, increasing gradually with latitude before becoming 1° poleward of 30°S and 30°N. In the vertical, the model has 40 layers with 27 layers in the upper 400 m. Its vertical resolution is 10 m from the surface to the 240-m depth and increases gradually to about 511 m in the lowest layer with a bottom depth of about 4.5 km. The land surface model in CFS is the two-layer model described in Mahrt and Pan (1984).

The atmospheric and oceanic components are coupled without flux adjustment, and the two components exchange time-averaged quantities once a day. Full atmosphere–ocean interaction is confined to 65°S–50°N, and the weighted average of observed and modeled sea surface temperatures (SSTs) is used for the latitudes poleward from this latitude band in the way that the SSTs at 65°S and 50°N equal those of the ocean model and the SSTs at 74°S and 64°N equal the observed climatology (see Saha et al. 2006 for details).

We analyze the output from the CFS retrospective predictions that cover all 12 calendar months from 1981 to 2003. These hindcast runs, each of which is a 9-month integration, are an ensemble of 15 members starting from perturbed real-time oceanic and atmospheric initial conditions (ICs) from the NCEP Global Ocean Data Assimilation (D. Behringer 2005, unpublished manuscript) and the NCEP/Department of Energy (DOE) Atmospheric Model Intercomparison Project II Reanalysis (R2) (Kanamitsu et al. 2002), respectively. In the 15 ensemble runs for a specific starting month (e.g., June), the ICs of days 9–13, 19–23, and the last two days of the previous month (e.g., May) and those of days 1–3 of the concurrent month (e.g., June) are used. Unless specified, the values of CFS presented in this paper are the ensemble means of 15 members, and the

climatological means are the time averages for 1981–2003.

The observed datasets used for model verification include the Climate Prediction Center Merged Analysis of Precipitation (CMAP) (Xie and Arkin 1996), winds and temperatures from the NCEP/DOE R2 (Kanamitsu et al. 2002), and the NOAA optimally interpolated (OI) SST analysis (Reynolds et al. 2002). We also analyze a long-period precipitation analysis developed by the Climate Prediction Center (Chen et al. 2002), that is, monthly precipitation reconstruction data over land and oceans (PREC) at a resolution of $2.5^\circ \times 2.5^\circ$ latitude/longitude for the time period from 1948 to present. The dataset contains gauge-based global observations and has been used in several investigations including studies of the Asian monsoon (Liang et al. 2007) and the variability of U.S. precipitation (Yang et al. 2007a). In addition to these commonly used products, we also use the observational dataset of monthly surface air temperature developed by Fan and Van den Dool (2008). This dataset, at $0.5^\circ \times 0.5^\circ$ latitude/longitude resolution, covers the global land areas for the period from 1948 to present. It is based on a combination of the Global Historical Climatology Network version 2 and the Climate Anomaly Monitoring System datasets.

3. Monsoon simulations

In this section, we discuss the results for zero-month lead (LM0) by referencing monsoon simulations to the CFS values for June–August (JJA) using the ICs of May and early June (see section 2 for specific dates). Figure 1 shows the JJA climatology of CMAP precipitation, CFS precipitation, and their difference. Figure 1a illustrates several centers of observed precipitation over western India, Bangladesh/Burma, the Indo-China Peninsula, the South China Sea (SCS), and east of the Philippines, with the highest center over Bangladesh, Burma, and the northern Bay of Bengal (BOB). It also shows large precipitation over the tropical central-eastern Indian Ocean (IO) and the meiyu rainband over eastern China, baiu over Japan, and changma over Korea. Furthermore, the figure shows relatively lighter precipitation over the eastern Indian coast, east of the Indo-China Peninsula, and the northwestern Pacific (owing to the influence of the subtropical high). Light precipitation is also seen over the western Arabian Sea where ocean upwelling driven by monsoon flow cools the sea surface.

Comparison between Figs. 1a and 1b indicates that the CFS captures the general features of observed precipitation quite well. For example, the model captures

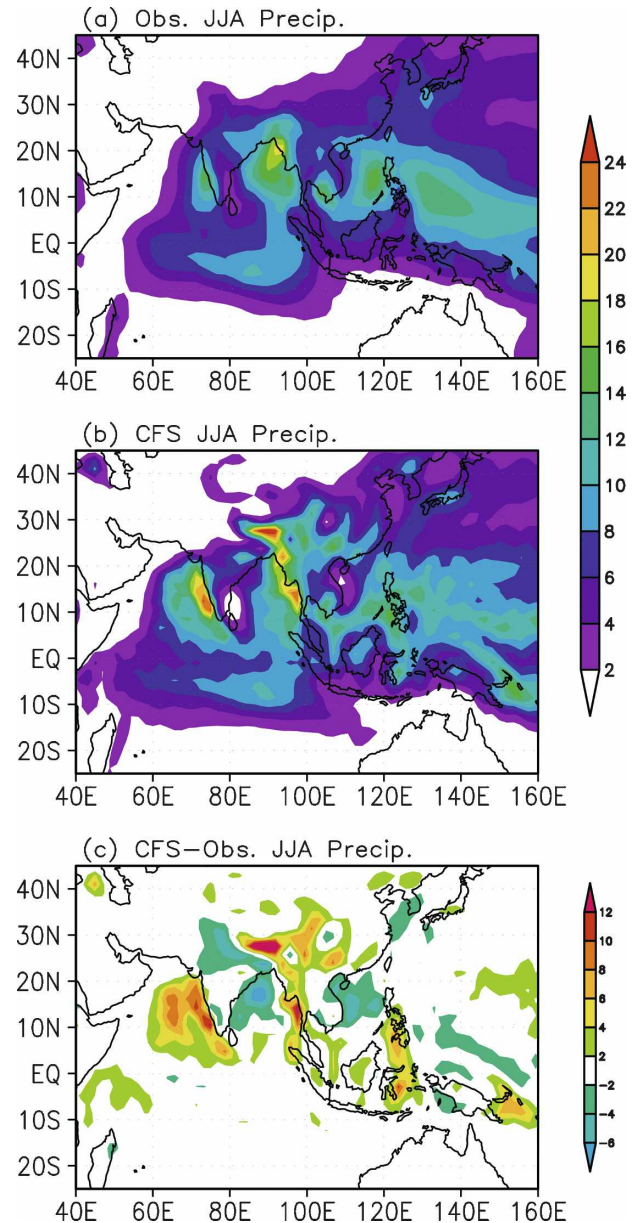


FIG. 1. The (a) 1981–2003 climatology of JJA precipitation from CMAP, (b) 1981–2003 climatology of JJA ensemble-mean precipitation from CFS (0-month lead), and (c) difference between (b) and (a). Units: mm day^{-1} .

the locations of major high and low centers of monsoon precipitation. The model precipitation and observed precipitation also compare reasonably well in magnitude in many places. A merit of the CFS appears in simulating the East Asian mei-yu rainband and the precipitation over the tropical IO. In particular, while general circulation models often fail to produce the mei-yu rainband or even generate relatively low precipitation over East Asia (see Kang et al. 2002), the CFS captures

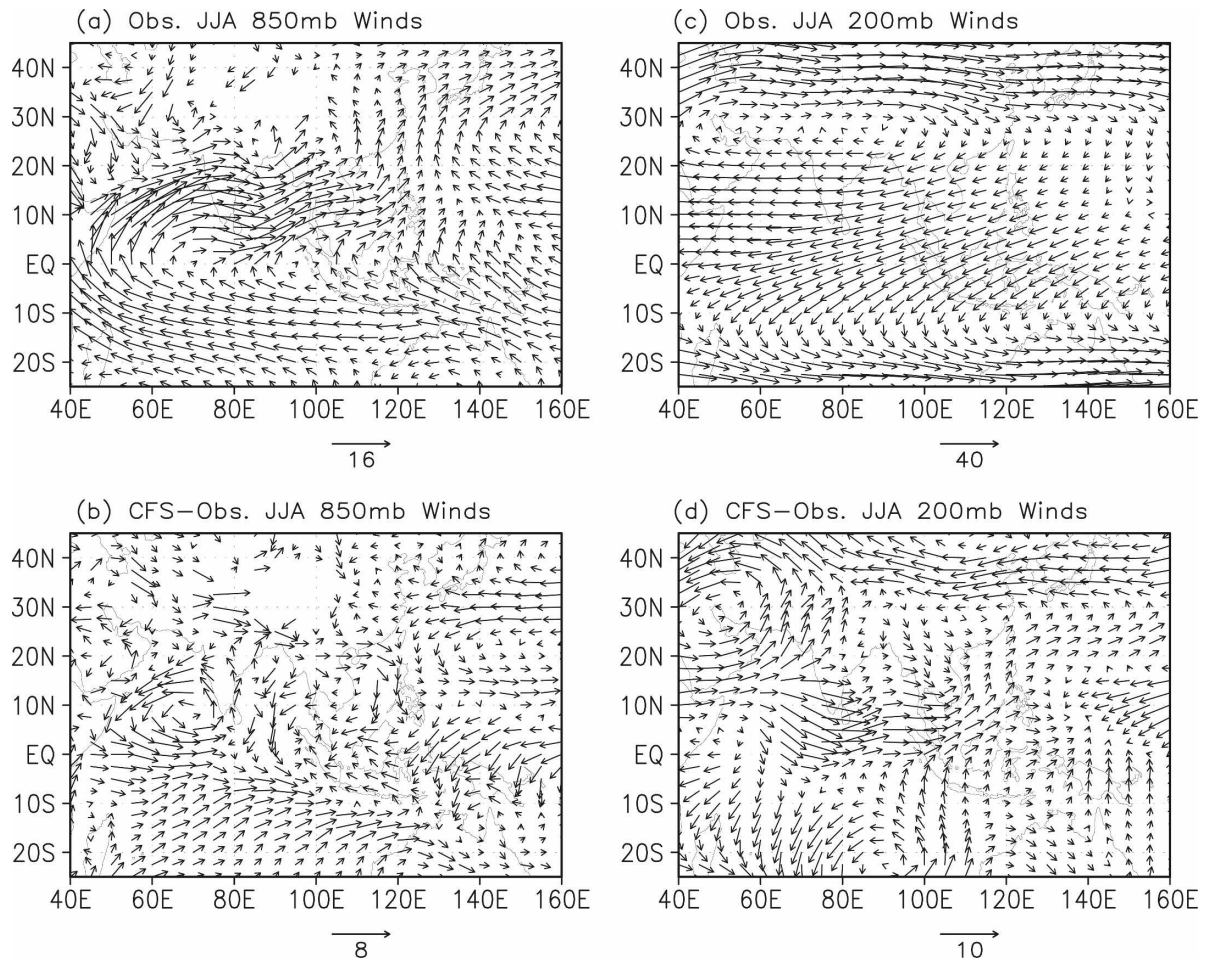


FIG. 2. The 1981–2003 climatology of JJA (a) 850-mb and (c) 200-mb winds from NCEP/DOE R2 and (b) differences between the climatological JJA ensemble-mean (b) 850-mb and (d) 200-mb winds from CFS (0-month lead). Units: m s^{-1} .

the phenomenon of precipitation reasonably well, in spite of an underestimation of precipitation over Korea and the Yellow Sea. The CFS performs well in capturing the tropical IO precipitation center, for which many models even fail in reproducing the shape or the orientation of the precipitation center (see Kang et al. 2002, Fig. 1). However, the CFS overestimates the precipitation over the eastern Arabian Sea, the Himalayas, and Burma and underestimates the precipitation over northwestern BOB, northern India, and SCS (see Fig. 1c). The overestimation of precipitation over the southern–southeastern hills of the Tibetan Plateau seems one of the main problems of monsoon simulations by the model. It should be pointed out that many major features of the CFS simulations remain similar in the longer lead time, which will be discussed in sections 4 and 5.

Figure 2 shows the reanalysis winds at 850-mb and 200-mb levels and the differences between the reanaly-

sis and CFS simulations. It reveals several major features of the observed monsoon including the lower-tropospheric southwest monsoon flow over tropical Asia, the cross-equatorial Somali jet, the northwest trade winds (Fig. 2a), the upper-tropospheric easterly monsoon flow, and the South Asian anticyclonic pattern (Fig. 2c). On the other hand, Fig. 2 also reveals several deficiencies of the model in simulating the monsoon circulation. In the lower troposphere, the southeasterly trade winds over the tropical IO, the Somali jet, and the subtropical northwestern Pacific high are weaker than the observed (Fig. 2b). In the upper troposphere, the easterly monsoon flow in the model is also too weak (Fig. 2d), associated with a weak South Asian high (e.g., at the 200-mb geopotential height; figure not shown). Overall, the CFS produces weaker-than-observed circulation patterns of the Asian summer monsoon. Furthermore, as shown in Figs. 2b and 1c, the deficiency of CFS in simulating the low-level

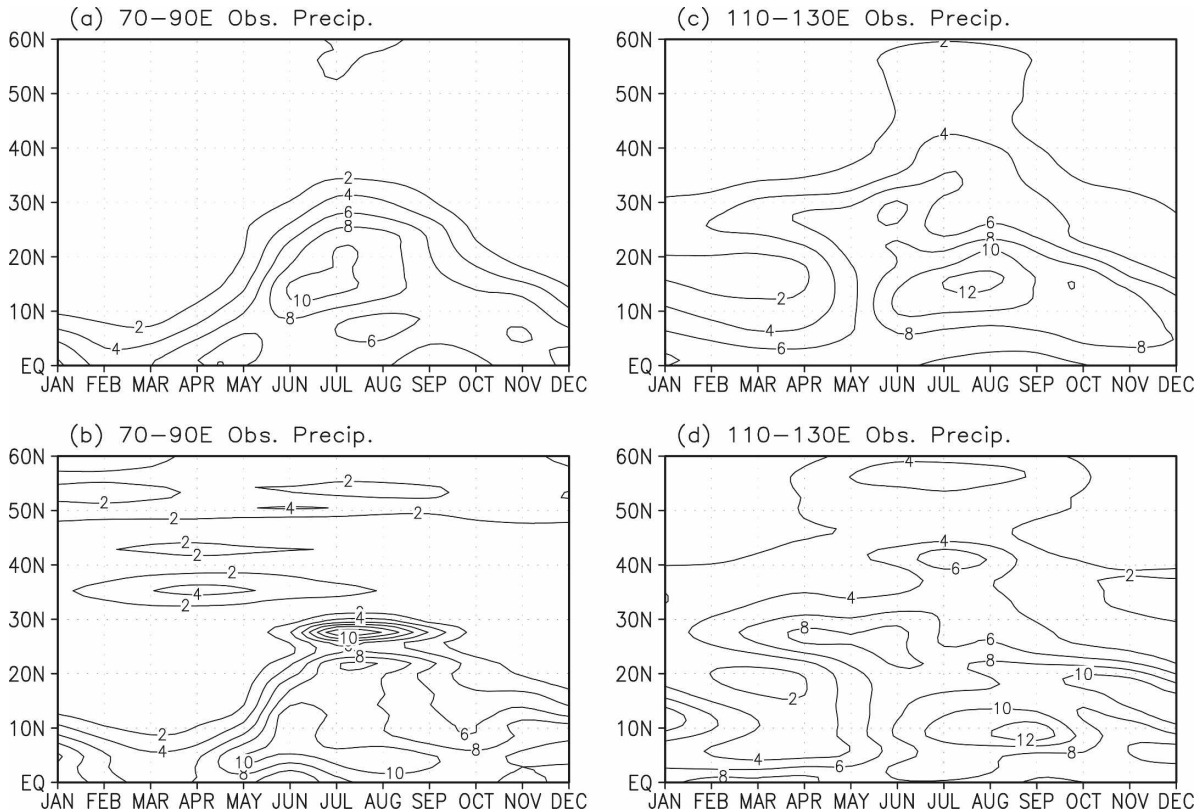


FIG. 3. (a) Time–latitude section of (a) climatological CMAP precipitation (mm day^{-1}) and (b) CFS ensemble-mean precipitation of 0-month lead along 70° – 90° E. (c) Time–latitude section of climatological CMAP precipitation and (d) the CFS ensemble-mean precipitation along 110° – 130° E.

monsoon flow, which leads to several differential cyclonic and anticyclonic patterns in the figure, is dynamically consistent with the shortcoming of the model in simulating monsoon precipitation.

To compare the evolution of CFS and observed monsoons, we plot the time–latitude cross sections of CMAP precipitation along 70° – 90° E for the Indian monsoon and 110° – 130° E for the East/Southeast Asian monsoon and the differences between CFS and CMAP precipitations along these longitude bands. Figure 3a indicates that the onset of Indian monsoon rainfall is characterized by a process in which heavy precipitation shifts gradually from the equator in spring to subtropical India in summer. The monsoon is fully developed in India in June, continues to shift northward (more gradually) thereafter, and withdraws quickly in September. In JJA when major monsoon precipitation is located over the Indian Subcontinent, the precipitation over tropical IO decreases before it reintensifies in September. In East–Southeast Asia, the monsoon onset exhibits a relatively more rapid process from May to June (Fig. 3c). Note that the longitude band for East–Southeast Asia includes the SCS where monsoon onset

is characterized by a “sudden jump” process in May (Lau and Yang 1997). Compared to the Indian monsoon, the East–Southeast Asian monsoon extends farther northward in summer and retreats southward more systematically in autumn. In addition, subtropical (20° – 30° N) premonsoon precipitation in springtime, resulting mainly from frontal systems, is apparent in Fig. 3c.

Figure 3 shows that the CFS captures the onset and intensity of Indian and East–Southeast Asian monsoons, as well as the premonsoon precipitation and the northern extent of the East–Southeast Asian monsoon, reasonably well. However, the model’s maximum precipitation in East–Southeast Asia is too far south and the retreat of the monsoon is not well captured for either India or East–Southeast Asia. The model deficiency in simulating the precipitation over the Tibetan Plateau emerges again from Fig. 3b. Overall, the CFS simulates the seasonal march of monsoon rainfall over Southeast–East Asia better than that over South Asia, which seems different from the simulations by some climate models (e.g., Lau and Yang 1996).

We further examine the variability of several commonly used dynamical monsoon indices, which include

the Webster–Yang monsoon index (WY) (Webster and Yang 1992), the South Asian monsoon index (SA) (Goswami et al. 1999), the Southeast Asian monsoon index (SEA) (Wang and Fan 1999), and the East Asian monsoon index (EA) (Lau et al. 2000). The WY index is defined as the vertical shear of zonal winds between 850-mb and 200-mb levels averaged over 0° – 20° N, 40° – 110° E; and the SA index the vertical shear of meridional winds between 850-mb and 200-mb averaged over 10° – 30° N, 70° – 110° E. The definitions for SEA and EA are U_{850} (5° – 15° N, 90° – 130° E) – U_{850} (22.5° – 32.5° N, 110° – 140° E) and U_{200} (40° – 50° N/ 110° – 150° E) – U_{200} (25° – 35° N, 110° – 150° E), respectively. The details of these monsoon indices have been discussed by Wang and Fan (1999), Lau et al. (2000), and Yoo et al. (2006). Figure 4 shows that the CFS simulates the interannual variability of WY, SA, and SEA very well. For these tropical monsoon components, the correlation between the model and observations is highly significant. The best simulation occurs for WY ($R = 0.77$), which shows a nearly one-to-one correspondence in the interannual variability between the modeled and observed values. However, the CFS consistently produces weaker-than-observed monsoon circulation measured by WY. This feature demonstrates a systematic error of the CFS in simulating the Asian summer monsoon. Furthermore, the CFS performs poorly in capturing the variability of the subtropical monsoon component measured by EA. As shown in Fig. 4d, the variability of modeled EA is unrealistically small. Nevertheless, this problem is not unique to the CFS, given the general difficulties in simulating the climate over East Asia by global climate models (Kang et al. 2002).

Both Figs. 2 and 4 indicate that the underestimation of monsoon intensity by the CFS is more serious for the large-scale monsoon than for regional monsoon features. This suggests a need to examine the large-scale temperature gradient, which plays a critical role in the evolution of the monsoon, especially the evolution of the South Asian high from spring to summer, and in the intensity of the summer monsoon circulation (Yang et al. 2004; Yang and Lau 2006). Figure 5a, which shows the difference in surface temperature between CFS (LM0) and R2, indicates a cold bias of CFS over the Asian continent. Except for the southern hills of the Tibetan Plateau and part of India, the temperature in CFS is mainly lower than that in R2. The cold bias over the Asian continent leads to a weaker temperature gradient between the continent and the neighboring Indo-Pacific Oceans. This feature of the cold bias is also confirmed by replacing the R2 temperature by the observed surface temperature (Fan and Van den Dool 2008) over land and by OI SST over oceans (Fig. 5b),

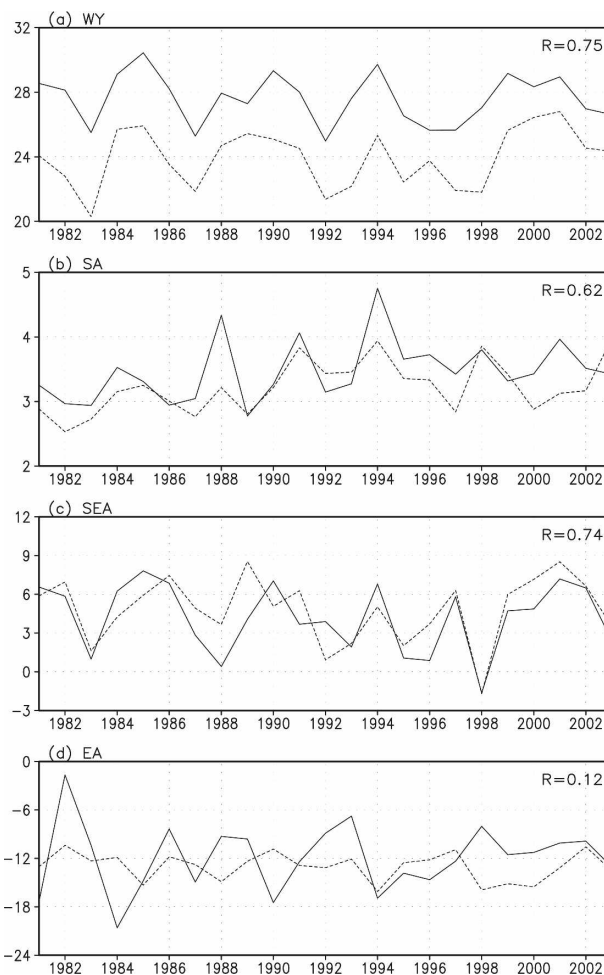


FIG. 4. Asian summer monsoon components, for both NCEP/DOE R2 and CFS (LM0) ensemble means, measured by various JJA dynamical monsoon indices: (a) WY monsoon index; (b) SA monsoon; (c) SEA monsoon; and (d) EA monsoon. Solid lines are for observations and dashed lines for CFS. Units: m s^{-1} .

although the observed surface air temperature shows more regional features. We have also examined the climatology and interannual variability of soil moisture and snow over the Eurasian continent in the CFS (figures not shown) and found that they are evidently different from the observed fields. Particularly, the two-layer land model used in the current operational NCEP CFS overestimates the soil moisture over the Tibetan Plateau and its adjacent regions, consistent with the overestimation of local precipitation (see Fig. 1c). It is anticipated that the four-layer Noah land surface model, a new version of the land model to be included in the next operational CFS, will improve the simulations and prediction of the Asian monsoon since it has demonstrated an overall improvement in precipitation and surface temperature simulations (Mitchell et al.

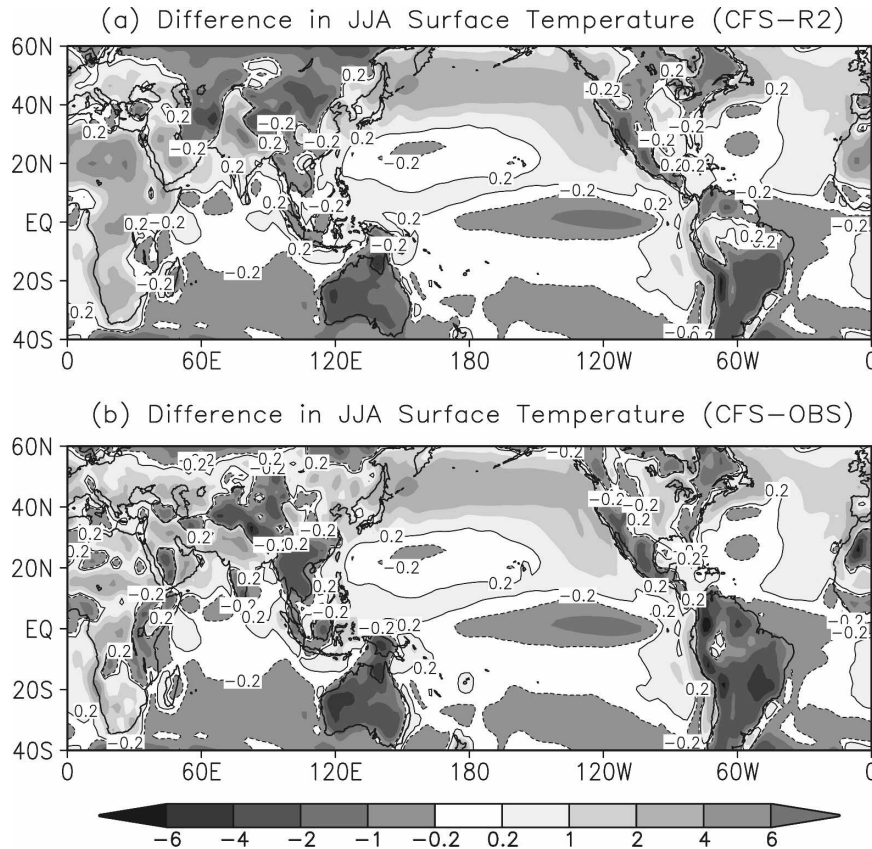


FIG. 5. (a) Difference in 1981–2003 climatological JJA surface temperature between CFS (LM0) and NCEP/DOE R2 in units of $^{\circ}\text{C}$; (b) as in (a) but the R2 temperature is replaced by OI SST over oceans and observed surface air temperature over land (Fan and Van den Dool 2008).

2006). Indeed, experimental hindcast simulations have shown that the four-layer Noah land surface model yields more realistic precipitation and atmospheric circulation patterns of the Asian summer monsoon than does the current two-layer model (S. H. Yoo et al. 2007, personal communication; available online at http://www.cpc.ncep.noaa.gov/products/outreach/proceedings/cdw32_proceedings/poster-sessions.shtml).

On the other hand, apparent warm bias occurs over Africa and the extratropical North Pacific. In particular, the warm bias over the North Pacific is associated with weaker-than-observed overlying westerlies. The impacts of these warm model biases on the simulations of Asian summer monsoon are relatively unclear. For example, the influence of extratropical Pacific SST on East Asian climate is considerably weaker than the effect of tropical northwestern Pacific SST, at least for the years 1993 and 1994 (Yoo et al. 2004). However, Yang et al. (1992) and Webster et al. (1998) have shown a connection between the atmospheric heat source over

southern Asia and the heat sink over tropical northern Africa through the lateral monsoon circulation, suggesting the importance of thermal contrast between Asia and Africa.

Figure 6 presents the meridional gradients of temperatures (MGT) of the troposphere and at the 850-mb, 500-mb, and 200-mb levels. It shows the observed values along latitude band 5° – 20°N and longitude band 40° – 120°E , as well as the differences between the CFS and observations. The observed MGT has been positive (warmer in the north than in the south) in the tropics since springtime and reaches a maximum between 10° and 30°N , west of 90°E , in July (Figs. 6a and 6c). As shown in Figs. 6b and 6d, the CFS MGT is consistently smaller than observed, except over 20° – 25°N in April and May. It should be pointed out that we have demonstrated a connection of the weak large-scale monsoon circulation to the small meridional gradient of temperature in the CFS. However, the large-scale features shown in MGT may not be linked closely to the

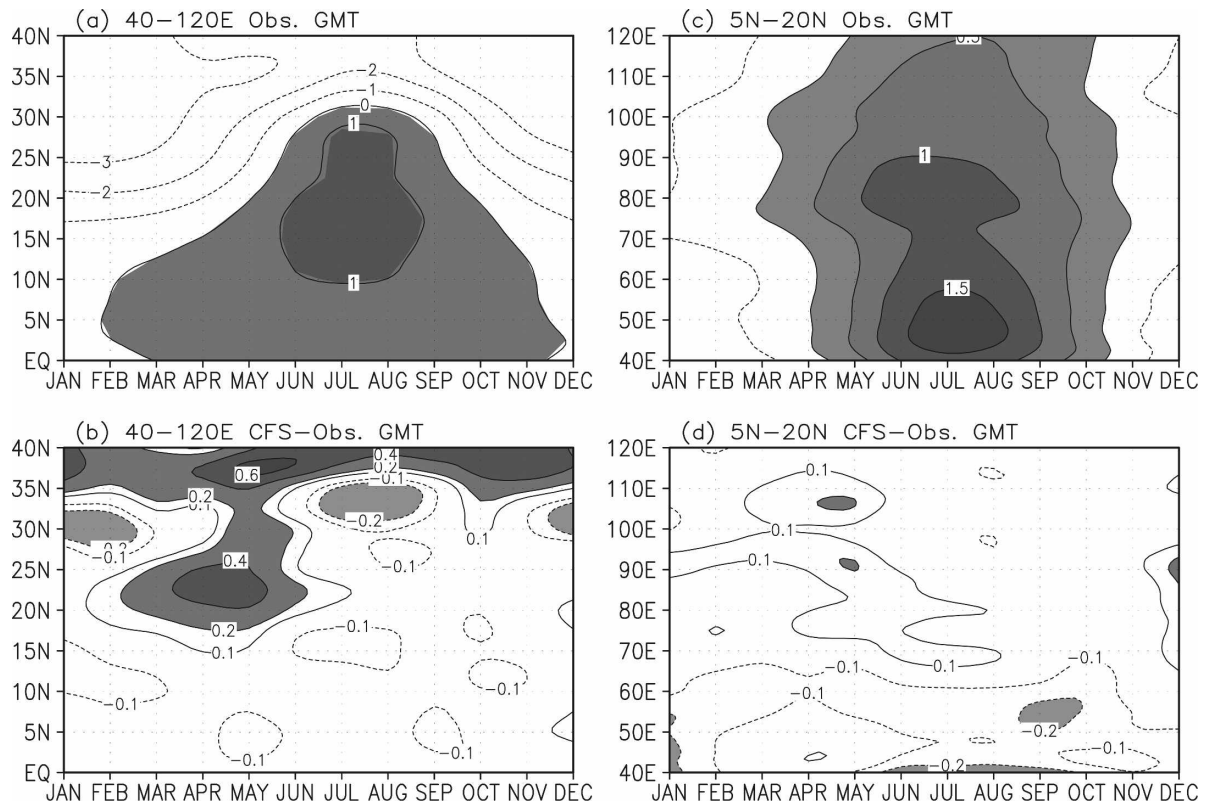


FIG. 6. (a) Time-latitude section of climatological meridional temperature gradient (MGT) ($^{\circ}\text{C}$ per 5° lat) along 40° – 120°E calculated from the NCEP/DOE R2. Temperature is the vertically integrated temperature at levels 850 mb, 500 mb, and 200 mb. (b) As in (a) but for the difference in MGT between CFS and R2. (c), (d) Similar to (a), (b) but for the time-longitude section along 5° – 20°N (MGT: $^{\circ}\text{C}$ per 5° lon).

precipitation patterns characterized by large regional features.

4. Monsoon predictions

To discuss monsoon predictions, we analyze the results for one month and longer leads (see section 2 for details about the ICs for each lead). Note that, in the hindcast products of the 9-month integration, the prediction of the 6-lead month (LM6) is the data of the longest lead month available for the analysis of seasonal-mean fields. For this study, the integration using the ICs of November and early December is the longest lead (LM6) for analysis of the JJA monsoon and, for brevity, we refer to these ICs for JJA monsoons as December ICs.

Figure 7 shows the JJA precipitation and 850-mb winds of CFS for a 1-month lead (LM1) using May ICs. Comparison between this LM1 lead and the LM0 lead indicates extraordinarily similar features of precipitation (Figs. 7a and 1b). Particularly, similar features also appear in the patterns of atmospheric circulation, al-

though the LM0 pattern is not shown explicitly in Fig. 2 for a direct comparison. Presenting Fig. 7 here is necessary because, in the subsequent discussions, we mainly discuss the results of monsoon prediction by comparing the CFS hindcasts of different lead months with both observations and LM1.

Figure 8 shows the differences in CFS precipitation between LM1 and LM0 (LM1 minus LM0, Fig. 8a), between LM2 and LM1 (LM2 minus LM1, Fig. 8b), and so on (here, a 2-month lead is defined as LM2, 3-month lead as LM3, and so on). From LM0 to LM1 (Fig. 8a) the largest changes are the precipitation deficits over the eastern Arabian Sea including the west India coast and the excessive precipitation over the equatorial western IO. These precipitation differences remain until LM4 and LM5, respectively. From LM1 to LM2 (Fig. 8b) the largest changes are the deficits over the tropical eastern IO and western Pacific including the northern Philippines. Since LM2, an overestimation of precipitation related to the IO dipole structure by CFS is apparent (see discussion for SST in Fig. 9). Other major features of Fig. 8 include the large error growth over the

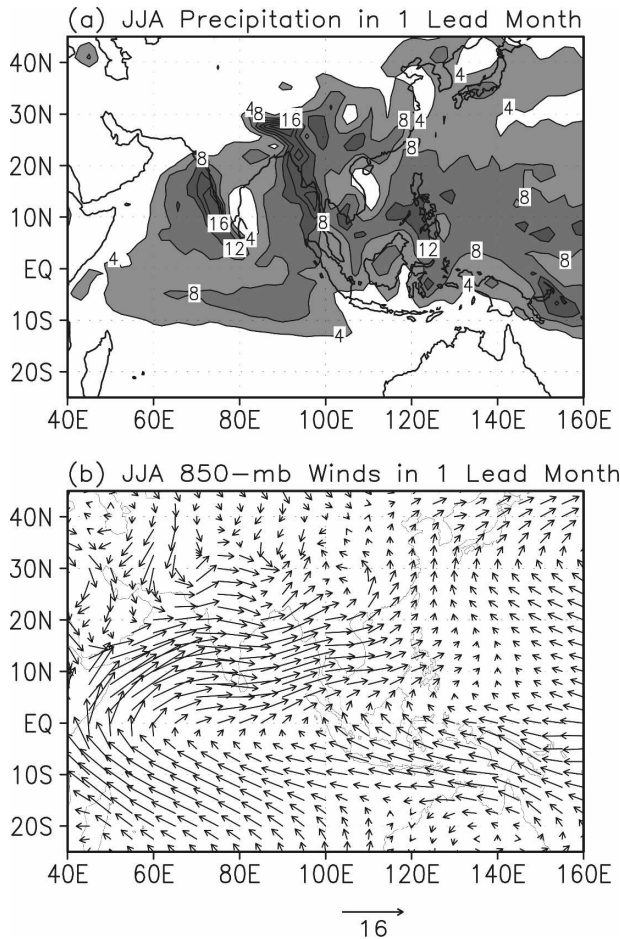


FIG. 7. Climatological patterns of precipitation (mm day^{-1}) and 850-mb winds (m s^{-1}) predicted by CFS with 1-month lead. The ensemble-mean values of 15 members are shown.

IO from LM4 to LM5 (Fig. 8e). Overall, the model bias changes with lead time more significantly over the IO than over the western Pacific. In addition, since the tropical western IO SST is strongly associated with Niño-3.4 SST and the eastern IO SST is significantly linked to the convection over the Maritime Continent (Wang et al. 2003; Yang et al. 2007b; Zhang and Yang 2007), the impact of ENSO on CFS simulation over IO, especially that shown by the earlier signal over western IO (compared to that over eastern IO), can be seen from Fig. 8. More about the impact of ENSO on CFS prediction of the Asian and Indo-Pacific climate is discussed in the following section.

Similarly, we show the differences in CFS SST and of 850-mb winds for different time leads in Fig. 9. In general, the surplus (deficit) differences shown in Fig. 8 are accompanied by warming (cooling) tendencies in Fig. 9. This feature is especially clear for the precipitation excess/warming tendency over the western IO and the

precipitation deficit/cooling tendency over the eastern IO. The relatively large changes in precipitation from LM2 to LM3 (Fig. 8c) and from LM4 to LM5 (Fig. 8e) are associated with the relatively large changes in SST (Figs. 9c and 9e). Note that precipitation over the extratropical North Pacific does not respond to SST changes significantly.

Figure 9 shows a remarkable feature in the southwesterly monsoon flow, the Somali jet, and the southeasterly trade winds over the tropical IO. That is, these monsoon-related wind patterns weaken with an increase in lead time. While the weakening of the Somali jet accounts for the warming over the western IO, the consistent weakening of the monsoon flow and trade winds explains the development and eastward extension of the intensifying warming tendency over the tropical northern and southern IO. Over the western North Pacific, a weakening tendency occurs in the subtropical high, especially to its southern flank, associated with a general cooling tendency.

Figures 8 and 9 indicate that the underestimation of monsoon circulation and the overestimation of IO-dipole-related features by the CFS are improved in the predictions using shorter-lead ICs. For example, Figs. 8e and 9e show large negative values over the tropical IO, meaning that the prediction using January ICs is closer to observation than is the prediction using December ICs. Overall, the model also performs significantly better when using the March ICs than the February ICs (Figs. 8c and 9c). However, differences are relatively smaller between the applications of ICs of November and December (Figs. 8f and 9f). Perhaps the more favorable feature shown in Figs. 8 and 9 is that the errors of monsoon prediction and the growth of these errors are small over the Asian continent, compared to those over the IO. However, it should be pointed out that, although the overall errors do not change significantly throughout most of the forecast leads, larger errors exist in monsoon simulations by the CFS (comparison of 0-month lead with observations) as seen in the last section.

We further assess the skill of prediction of the various dynamical monsoon indices discussed previously in Fig. 4. It can be seen from Fig. 10 that the CFS is highly skillful in predicting the large-scale Asian summer monsoon circulation, as seen in the confidence of predicting the monsoon measured by the WY index, which exceeds the 99% confidence level ($R = 0.52$, Student's t test) using the ICs of January (LM4) and the 95% level ($R = 0.41$) using the ICs of December (LM5). The Southeast Asian monsoon can be predicted at the 99% confidence level using the ICs of April and at the 95%

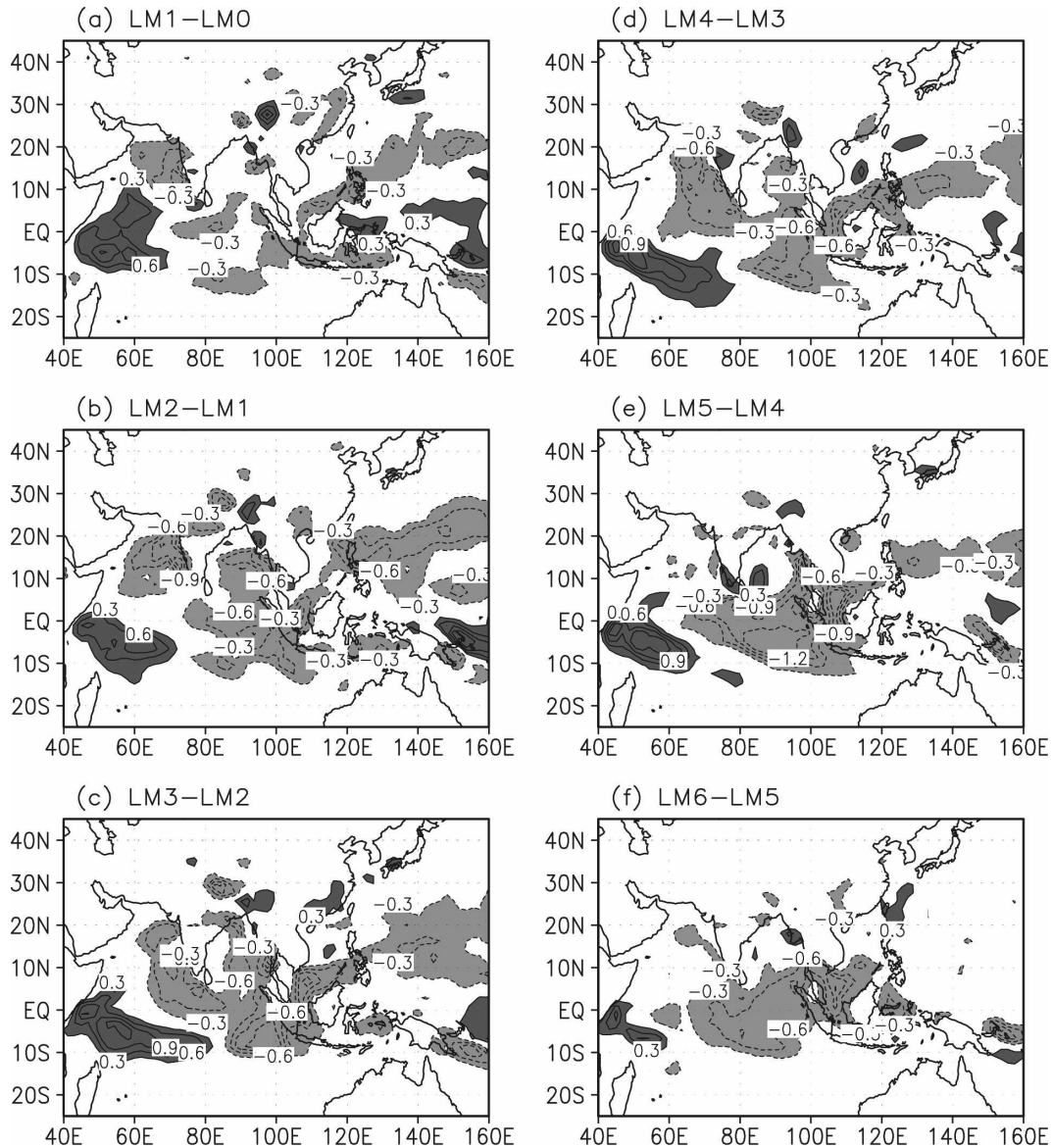


FIG. 8. Changes in CFS climatological JJA precipitation (mm day^{-1}) for different lead months: Pattern difference (a) difference between 1-month and 0-month lead and (b) between 2-month and 1-month lead, and so on.

confidence level using the ICs of March. (The confidence level exceeds 90% if the ICs of December are used.) In addition, the South Asian monsoon is also predictable at the 95% confidence level using the ICs of April. However, no skill is found in predicting the East Asian monsoon except the high correlation in LM5, which may appear erratically.

5. ENSO and skill of monsoon prediction

The NCEP model has exhibited reasonably high skill in simulating and predicting ENSO events and ENSO-

related climate signals (Peng and Kumar 2005; Wang et al. 2005; Saha et al. 2006). Here, we measure the skill of monsoon prediction by ENSO, focusing on the ability of the model in capturing the significant difference in SST, precipitation, and winds between warm and cold events, although ENSO and its climate influence may be asymmetric (An and Jin 2004; Cai et al. 2004). Figure 11 shows the composite pattern of SST difference between warm and cold events (warm minus cold) for the onset or development years of ENSO. In observations (Fig. 11a), positive SST anomalies are organized over the tropical central Pacific accompanied by nega-

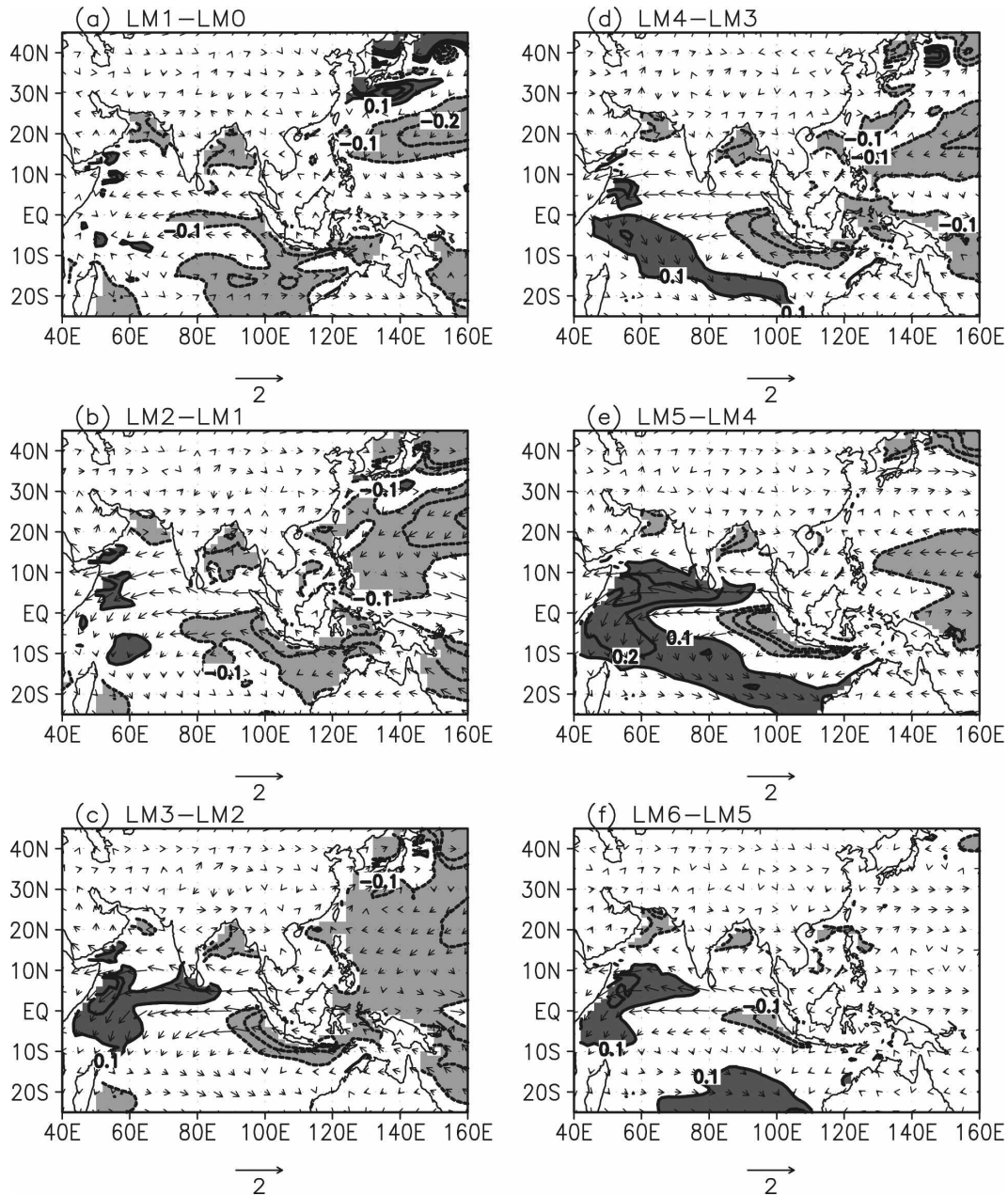


FIG. 9. As in Fig. 8 but for 850-mb winds (m s^{-1} ; vectors) and SST ($^{\circ}\text{C}$; shading).

tive anomalies over the western Pacific and southeastern IO. These SST anomalies including the longitudinal extent of warming SST anomalies over the tropical central Pacific are predicted by the CFS successfully. Although the model overestimates the amplitude of SST anomalies (Fig. 11b), it forecasts the Pacific SST anomalies at least four months ahead (Fig. 11f) and the eastern IO SST anomalies two months in advance (Fig. 11d). Nevertheless, the model tends to overpredict the negative SST anomalies over the northwestern Pacific,

outside the Philippine Sea. Another apparent problem existing in CFS is that, over the tropical eastern Pacific (east of 120°W), the SST is too high (low) during the El Niño (La Niña) years. This problem appears from the LM5 lead using the ICs of December and January (Fig. 11g).

Figure 12 shows the differences in precipitation and in 850-mb winds between the warm and cold events. Distinct features in the observed precipitation include the increase in precipitation over the tropical central

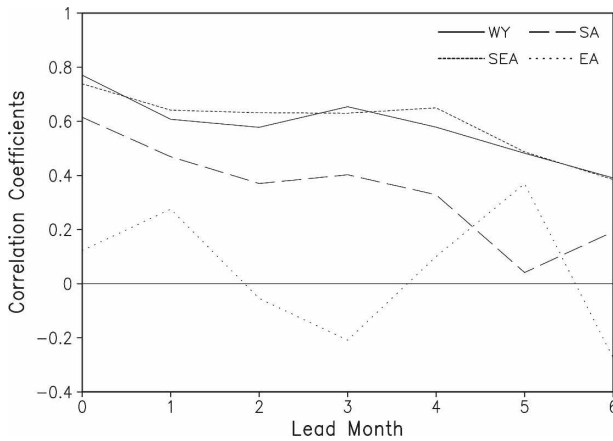


FIG. 10. The coefficients of correlation between the CFS predicted and observed monsoons for different lead months. Values are shown for different dynamical monsoon indices.

Pacific and the decrease in precipitation over the tropical eastern IO and Indonesia (Fig. 12a). Associated with these features is the weakening of tropical trade winds over the tropical Pacific. Over southern Asia, westerly monsoon flow intensifies near 15°N , especially

over Southeast Asia, causing divergence over SCS and its west. Figure 12b indicates that the CFS captures the main features of observed precipitation and winds described above. However, the signals in CFS winds appear too strong and too latitudinally extensive, and the model overestimates the changes in winds over the tropical southern IO and in precipitation over the southern Philippine Sea (near 10°N). Overall, the CFS is able to reasonably predict the ENSO-related precipitation and circulation anomalies three–four months in advance.

It can be seen from Fig. 13, which shows the composite patterns of SST difference between the warm and cold events for ENSO decay years, that the CFS also has larger skill in predicting the SST anomalies for the decay years of ENSO. Surprising skill is seen over the IO where the positive anomalies are predicted realistically at all time leads displayed. The outstanding performance of CFS in predicting the SST anomalies over the smaller SCS domain is also somehow unanticipated. These features indicate that the CFS captures and predicts the impact of ENSO on IO and SCS well. Over the Pacific, the model is able to predict the SST anomalies after ENSO peaks in LM5. However, the

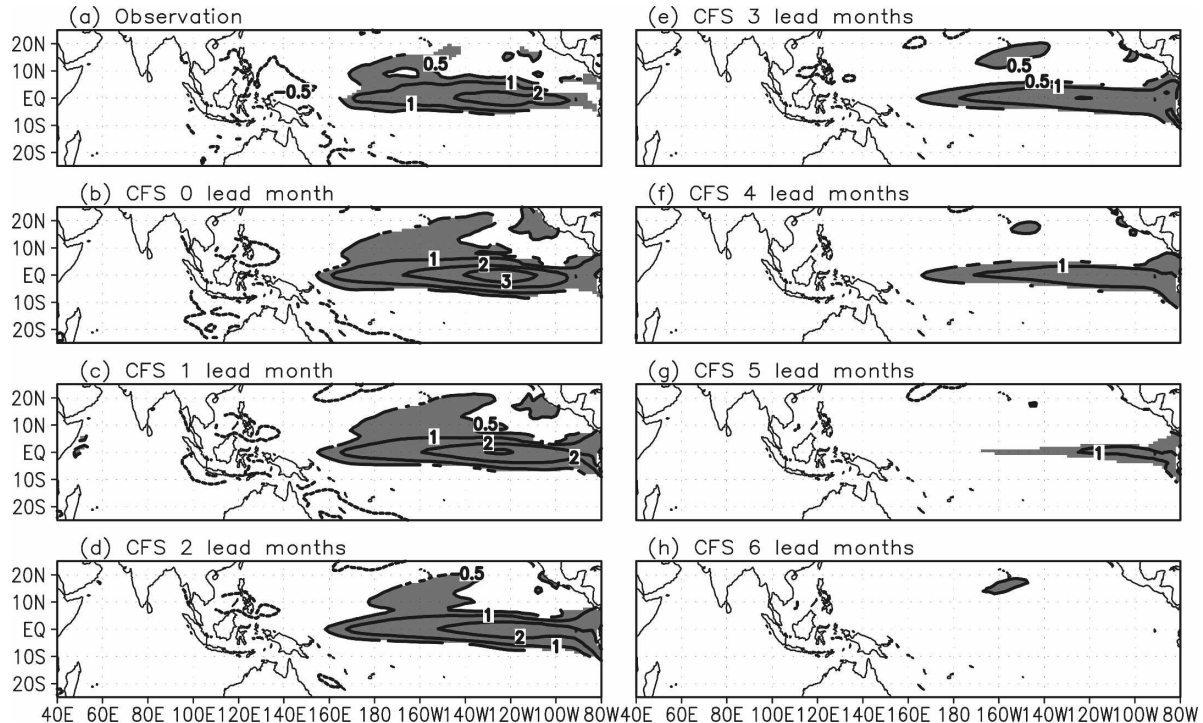


FIG. 11. Differences in JJA SST between warm and cold years (warm minus cold) of ENSO developing stage for (a) observations and (b)–(h) CFS ensemble means for different lead months. The warm years include JJA of 1982, 1986, 1991, 1994, 1997, and 2002, and the cold years include JJA of 1984, 1988, 1995, 1998, 1999, and 2003. Significant values exceeding the 95% confidence level of t test are shaded.

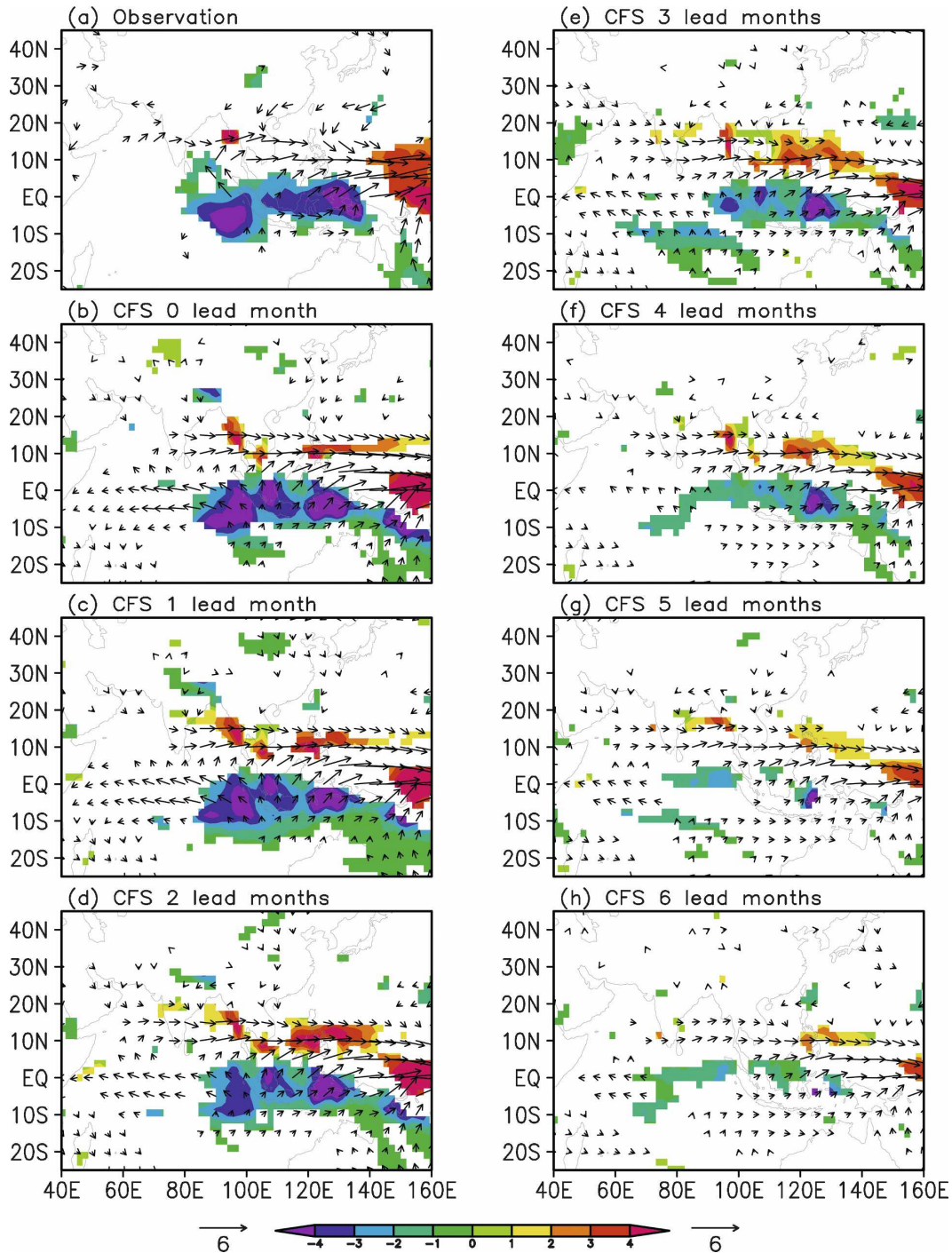


FIG. 12. As in Fig. 11 but for precipitation (shading) and 850-mb winds (vectors). Significant values exceeding the 95% confidence level of *t* test are shaded, or drawn for the vectors.

positive values over the tropical central-eastern Pacific in the LM6 lead (Fig. 13h) are unexpectedly larger than the observed.

Several important features are observed about the impact of ENSO on precipitation and atmospheric cir-

culatation from Fig. 14a. In the summers after El Niño, an anomalous anticyclonic pattern appears over the tropical northwestern Pacific. This atmospheric pattern forms and evolves with ENSO and conveys ENSO's impact on the climate over Southeast and East Asia

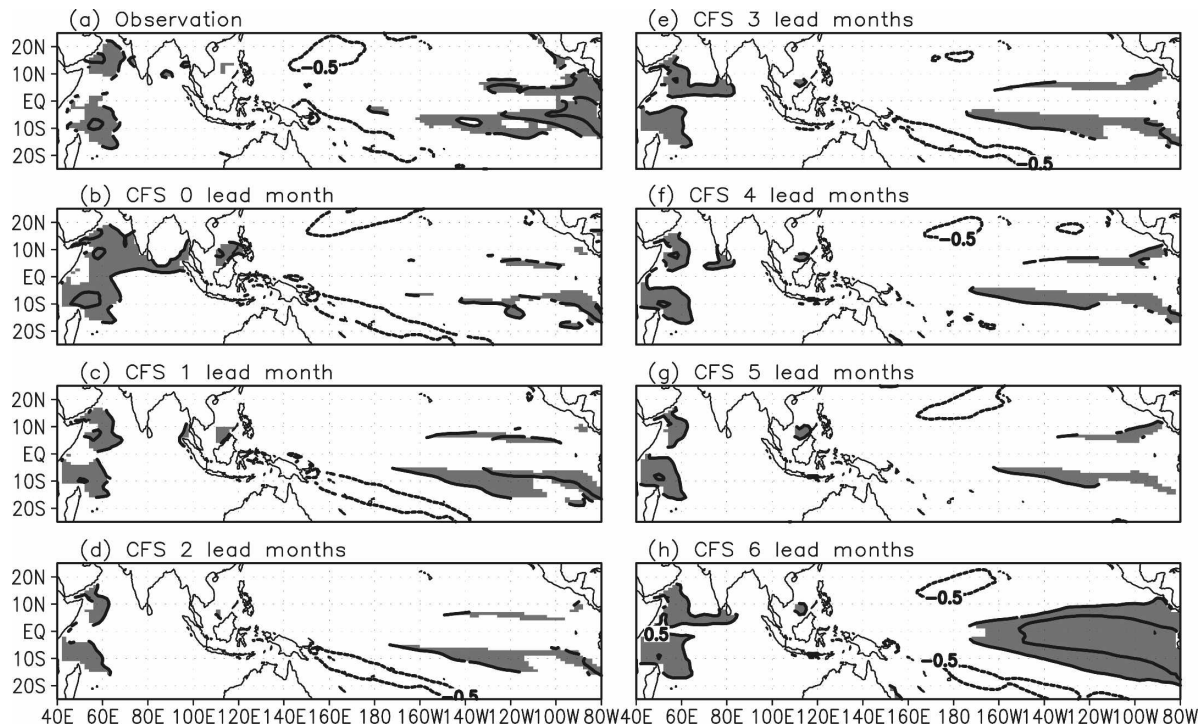


FIG. 13. Differences in JJA SST between warm and cold years (warm minus cold) of ENSO decaying stage for (a) observations and (b)–(h) CFS ensemble means for different lead months: warm years include JJA of 1983, 1987, 1992, 1995, 1998, and 2003 and cold years include JJA of 1985, 1989, 1996, and 2001. Significant values exceeding the 95% confidence level of t test are shaded.

(Wang et al. 2000; Lau et al. 2004). It is accompanied by a decrease in precipitation over the western Pacific. Over southern Asia and the IO, the westerly monsoon flow weakens, and the diminished Somali jet is associated with a precipitation increase over the tropical western IO, associated with the warm SST shown in Fig. 13. Since the CFS overestimates the impact of ENSO as discussed previously, the signals in precipitation and winds are more prominent in the model (Fig. 14b) than in observation. Nevertheless, the CFS predicts the ENSO-related changes (in precipitation and winds) in the decay years of ENSO several months ahead. More specifically, the CFS shows substantial skills in predicting the anomalous western Pacific anticyclone, the diminution of southern Asian monsoon flow, and the decrease in precipitation over the northwestern Pacific after the peaks of ENSO at lead time of several months.

Note that Liang et al. (2008) have applied a maximum signal-to-noise empirical orthogonal function (MSN EOF) analysis to depict the most predictable patterns of the Asian and Indo-Pacific climate in the NCEP CFS. The analysis optimizes the signal-to-noise ratio; that is, the leading modes maximize the ratio of the variance of ensemble mean (the signal) to the deviation among ensemble members (the noise). In a

moderate ensemble size of 15 members, the tool minimizes the effects of noise effectively [see Allen and Smith (1997) for details of the MSN EOF]. The patterns of precipitation, winds, and SST shown in Figs. 11 and 12 for the development years of ENSO are similar to the patterns of the first MSN EOF modes, and those shown in Figs. 13 and 14 for the decay years of ENSO are similar to the patterns of the second MSN EOF modes. This feature suggests that a significant portion of the skill of CFS in predicting the Asian and Indo-Pacific monsoon climate comes from the influence of ENSO.

We further examine the relationship between SST and the Webster–Yang monsoon index, which measures the thermally driven features of the broad-scale monsoon over tropical Asia and is successfully simulated and predicted by the CFS. In NCEP/DOE reanalysis (R2, Fig. 15a), the strong monsoon is associated with cooling over the tropical central–eastern Pacific and the northern IO and with warming over the northwestern and tropical-western Pacific. The condition over the Pacific is that a strong monsoon is connected to a La Niña event. Figure 15a also presents a strong link between the monsoon and IO SST and shows that the strong monsoon is related to a large meridional temperature gradient between the IO and

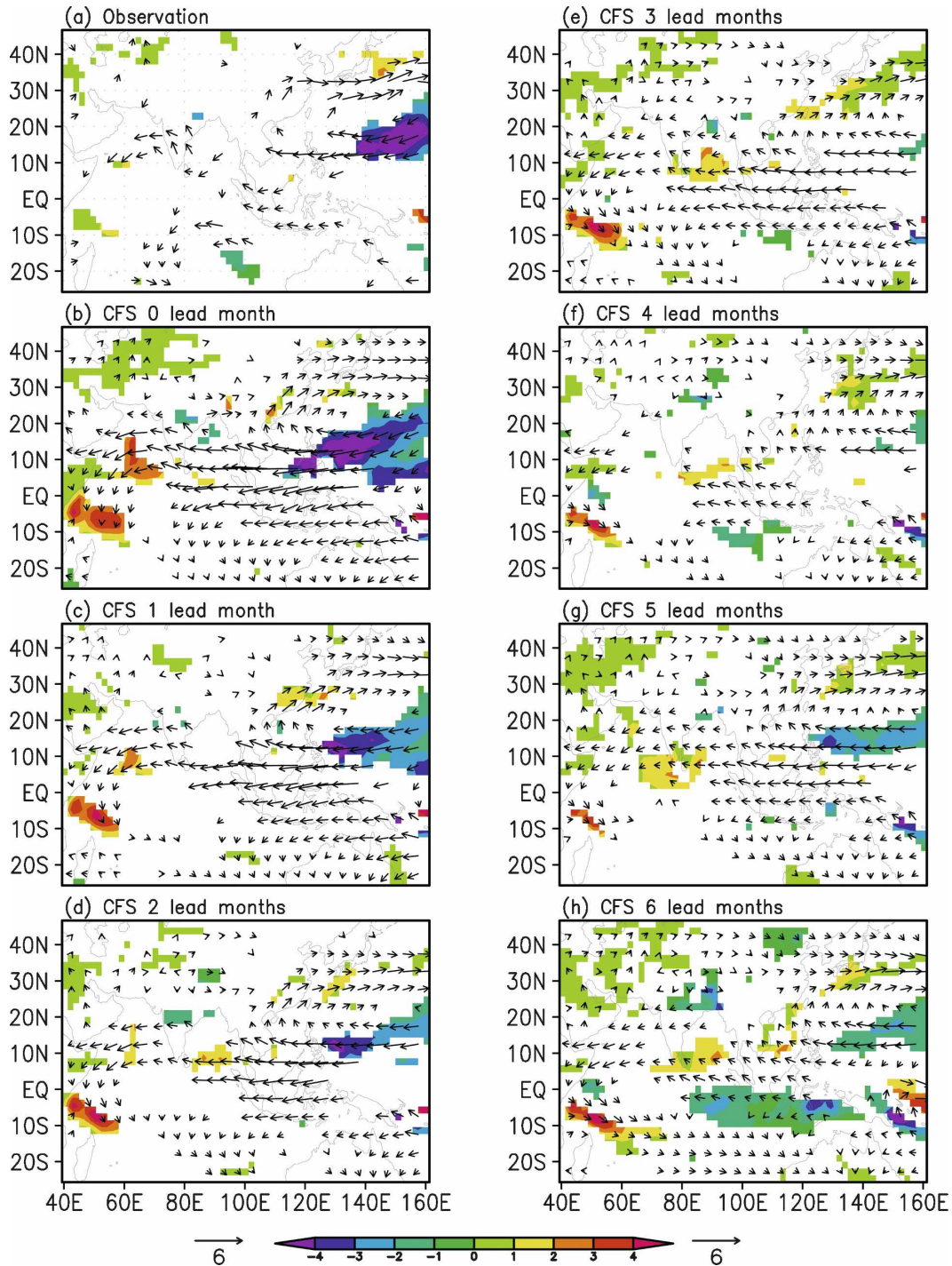


FIG. 14. As in Fig. 13 but for precipitation (shading) and 850-mb winds (vectors).

the Asian continent. The above features are confirmed by the correlation pattern in which the R2 surface temperature is replaced by the observed surface air temperature over land and IO SST over oceans (Fig. 15b).

The monsoon–ENSO relationship in CFS (Fig. 15c)

is, in general, similar to the patterns shown in Figs. 15a and 15b, especially in terms of the positive and negative signs of the correlation patterns. In particular, in both CFS and observations, the strong monsoon is associated with warming over the Asian continent and cool-

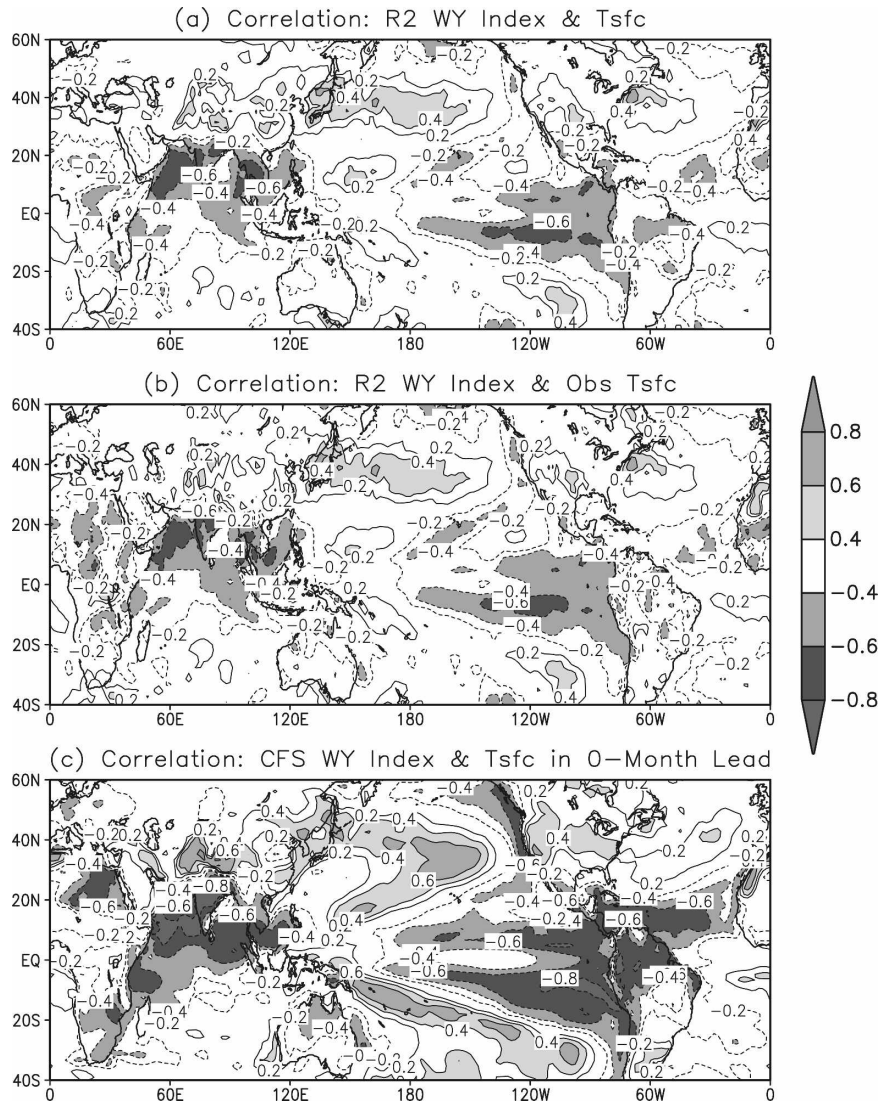


FIG. 15. (a) Correlation pattern between observed JJA Webster–Yang monsoon index and gridpoint surface temperature from R2; (b) as in (a) but for the IO SST over oceans and observed surface air temperature over land (Fan and Van den Dool 2008) and (c) for CFS LM0.

ing over the IO, or large meridional temperature gradient between the ocean and the continent. This characteristic further portrays the feature discussed previously: the weak mean Asian monsoon circulation in CFS (compared to observations) is related to a smaller meridional temperature gradient in the model. However, Fig. 15c also clearly shows that the SST–monsoon relationship in CFS is much stronger than observed, demonstrating again that, in the CFS, the connection of ENSO to the Asian and Indo-Pacific monsoon climate is too strong. The overly strong effect of ENSO on Asian monsoon simulation and prediction by the model is, in general, consistent with the results of Hu and Huang (2007) and Misra and Zhang (2007),

who showed that the skills of the CFS in predicting the climate over the tropical Atlantic Ocean and Brazil mainly come from the impact of ENSO.

6. Increase in model resolution and improvement of monsoon simulations

For years, the NCEP operational model (currently CFS T62) has been under continuing development to improve model performance. One of the main features of recent model development is the increase in horizontal resolution from T62 to 126 waves (T126). As shown previously (e.g., Sperber 1994; Cherchi and Navarra 2007), simulations of the Asian monsoon are sen-

sitive to the horizontal resolutions of numerical models, in both AMIP-type simulations and ocean–atmosphere coupled experiments. Although the T126 version has not been implemented in operational climate prediction at present, several free runs using the model have been conducted for model assessment purposes. Here, we compare the results from the free runs using two different resolutions, T62 and T126, to assess the impact of the model solution of monsoon simulations. Different from the hindcast experiments, in the free runs, integrations were performed continually for 50 years using the T62 and 100 years using the T126. Results for the last 45 years are analyzed for the purpose of comparison in this study. Note that comparison of hindcast experiments is not possible for this study because of the unavailability of a T126 hindcast.

Figures 16a–c show the climatological patterns of observed precipitation and 850-mb winds for JJA and the difference in precipitation and winds between CFS and observations. Over the Asian continent, the CFS T62 has difficulties in simulating the precipitation near the Tibetan Plateau (Fig. 16b). It underestimates the precipitation over northern India and overestimates the precipitation over western China. As discussed for the hindcast experiments in the previous sections, the model produces a weaker-than-observed mean monsoon circulation. These problems can still be seen in the free runs, but become less serious in T126 than in T62 (compared Figs. 16b and 16c). However, in contrast to this improvement, the simulation of the JJA precipitation over tropical IO is not improved from T62 to T126.

More apparent improvement in precipitation and atmospheric circulation simulations from T62 to T126 can be found for September–November (SON) (Figs. 16d–f). Figures 16e, f indicate an improvement in SON precipitation simulation over western and eastern Asia including India and China. The largest improvement occurs over the tropical IO. For example, the CFS T62 has difficulty in simulating the zonal dipole structure and its associated atmospheric circulation near the equator. In T126, the dipole structure has been simulated much more realistically, as reflected by the smaller model–observation differences in precipitation and winds. It is found that the SSTs over both the eastern and western IO are also simulated more realistically in T126 (figures not shown). The variability of the eastern IO SST, a more active pole of the IO dipole than the western IO SST, is sensitive to the convection activity and the response of atmospheric circulation over Southeast Asia. Within this context, the coupled ocean–atmosphere process over the Indian Ocean is thus better simulated in T126, compared to T62.

Figure 17 shows the standard deviations of the JJA

and SON observed precipitation and their differences from the CFS values. The centers of large deviation are generally collocated with the centers of heavy mean precipitation. Large values appear over western India, north of the BOB, southern China, the Philippines, and the western Pacific in JJA and over the SCS, western Pacific, and tropical eastern IO in SON. Improvement from T62 to T126 in capturing precipitation variability by the CFS can be seen near the Tibetan Plateau in JJA and over the tropical and northern IO in SON (except off Sumatra). Since the T126 version of CFS is considered the next version of the operational model of climate forecast at NCEP, the improvement in simulating the Asian monsoon and the IO zonal dipole structure by CFS T126 shown in Figs. 16 and 17 suggests better predictions of the Asian and Indo-Pacific monsoon climate by the next-generation operational model, which is expected to be implemented in 2010.

7. Summary

The NCEP operational Climate Forecast System provides monthly and seasonal climate predictions over the world, and CFS products are now becoming an important source of information for regional climate predictions in many Asian countries where a monsoon climate dominates. In this study, we have provided a comprehensive assessment of the performance of the model in simulating and predicting the Asian and Indo-Pacific summer monsoon climate, focusing on seasonal-to-interannual time scales.

The CFS successfully simulates many major features of the climatology and interannual variability of the Asian summer monsoon including centers of heavy monsoon precipitation and atmospheric circulation systems. It simulates the onset of the monsoon more accurately than the retreat of the monsoon and simulates the seasonal march of monsoon rainfall over Southeast Asia more realistically than that over South Asia. The CFS is skillful in predicting the major anomalous patterns of the Asian summer monsoon precipitation and the associated interactive oceanic–atmospheric processes at leads of several months. The model performs better in predicting the large-scale monsoon measured by the Webster–Yang index than other regional monsoon components. Overall, the skill of monsoon prediction by the CFS mainly comes from the impact of ENSO. However, the model produces weaker-than-observed large-scale monsoon circulation, due to the cold bias over the Asian continent, among other factors. It has difficulties in realistically simulating the precipitation over the Tibetan Plateau. In addition, the CFS tends to overestimate the magnitude of ENSO-related SST anomalies and to exaggerate the connec-

Precip and 850-mb Wind

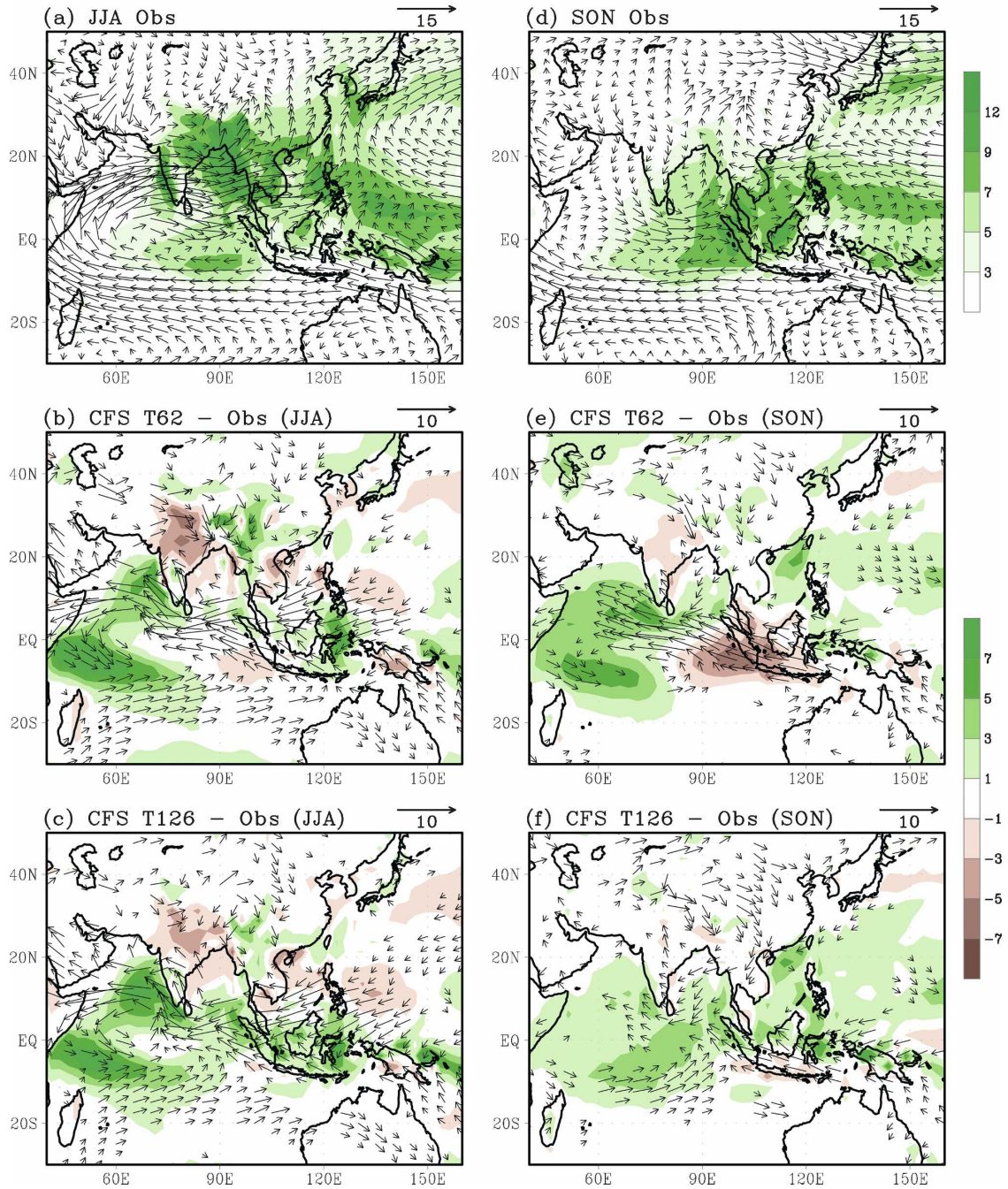


FIG. 16. The 1951–2005 climatological patterns of PREC precipitation (Chen et al. 2002) and 850-mb winds (NCEP–NCAR reanalysis) for (a) JJA and (d) SON. Differences in precipitation and winds (b), (e) between CFS T62 and observations and (c), (f) between CFS T126 and observations. The climatologies of 45 years are used for CFS.

tion of ENSO to the Asian monsoon and the impact of ENSO on the climate over Asia and the Indo-Pacific Oceans.

A higher-resolution version of the model, CFS T126, captures the climatology and variability of the Asian

monsoon more realistically compared to CFS T62. The largest improvement occurs to the simulations of precipitation near the Tibetan Plateau and over the tropical Indian Ocean associated with the zonal dipole structure. The analysis suggests that the NCEP's next opera-

Standard Deviation of Precip

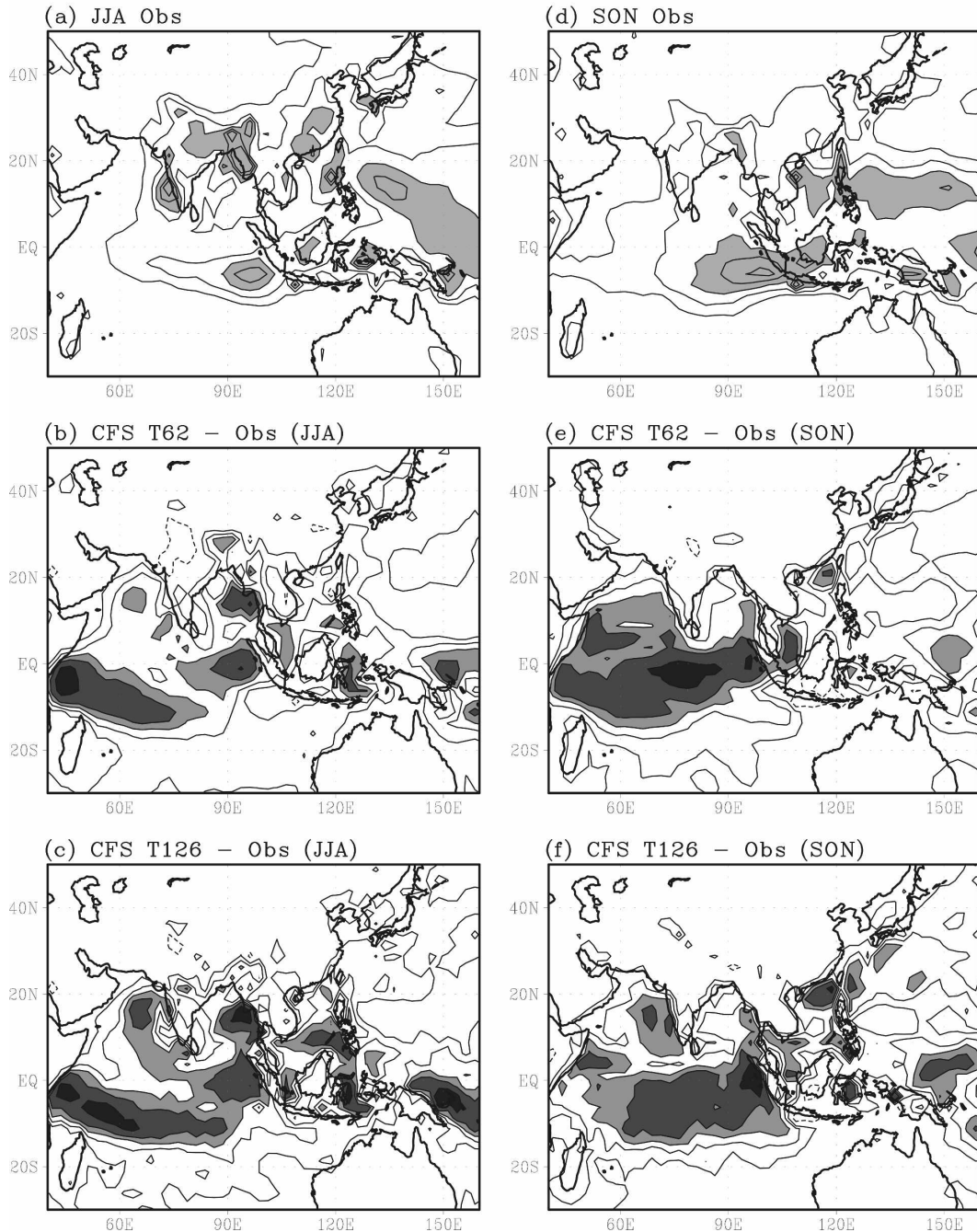


FIG. 17. Standard deviation of observed (left) JJA and (right) SON precipitation and their difference between CFS and observations for 45 years (see Fig. 16). Contour levels are (a), (d) 0.5, 1, 1.5, 2, and 2.5 and (b), (c), (e), (f) -0.5 , 0.5 , 1 , 1.5 , 2 , and 3 . Solid (dashed) contours are for positive (negative) values.

tional CFS T126, expected to be implemented in 2010, may simulate and predict the climate over Asia and the Indo-Pacific Oceans more realistically.

Acknowledgments. Zuqiang Zhang and Jianyin Liang, partially supported by the U.S. National Oceanic

and Atmospheric Administration and the China Meteorological Administration bilateral program on climate and monsoons, thank NOAA's Climate Prediction Center for hosting their visits while this study was conducted. Dr. Krishna Kumar provided constructive comments on an earlier version of the manuscript. The

comments by two anonymous reviewers and editor David Straus improved the overall quality of the paper.

REFERENCES

- Allen, M. R., and L. A. Smith, 1997: Optimal filtering in singular spectrum analysis. *Phys. Lett.*, **234**, 419–428.
- An, S., and F. Jin, 2004: Nonlinearity and asymmetry of ENSO. *J. Climate*, **17**, 2399–2412.
- Annamalai, H., S. P. Xie, and J. P. McCreary, 2005: Impact of Indian Ocean sea surface temperature on developing El Niño. *J. Climate*, **18**, 302–319.
- Blanford, H. F., 1884: On the connexion of Himalayan snowfall with dry winds and seasons of drought in India. *Proc. Roy. Soc. London*, **37**, 3–22.
- Cai, W., M. J. McPhaden, and M. A. Collier, 2004: Multidecadal fluctuations in the relationship between equatorial Pacific heat content anomalies and ENSO amplitude. *Geophys. Res. Lett.*, **31**, L01201, doi:10.1029/2003GL018714.
- Chen, M., P. Xie, J. E. Janowiak, and P. A. Arkin, 2002: Global land precipitation: A 50-yr monthly analysis based on gauge observations. *J. Hydrometeorol.*, **3**, 249–266.
- Cherchi, A., and A. Navarra, 2007: Sensitivity of the Asian summer monsoon to the horizontal resolution: Differences between AMIP-type and coupled model experiments. *Climate Dyn.*, **28**, 273–290.
- Fan, Y., and H. Van den Dool, 2008: A global monthly land surface air temperature analysis for 1948–present. *J. Geophys. Res.*, **113**, D01103, doi:10.1029/2007JD008470.
- Goswami, B. N., B. Krishnamurthy, and H. Annamalai, 1999: A broad-scale circulation index for interannual variability of the Indian summer monsoon. *Quart. J. Roy. Meteor. Soc.*, **125**, 611–633.
- Hu, Z.-Z., and B. Huang, 2007: The predictive skill and the most predictable pattern in the tropical Atlantic: The effect of ENSO. *Mon. Wea. Rev.*, **135**, 1786–1806.
- Kanamitsu, M., W. Ebisuzaki, J. Woollen, S.-K. Yang, J. J. Hnilo, M. Fiorino, and G. L. Potter, 2002: NCEP–DOE AMIP-II Reanalysis (R-2). *Bull. Amer. Meteor. Soc.*, **83**, 1631–1643.
- Kang, I.-S., and Coauthors, 2002: Intercomparison of the climatological variations of Asian summer monsoon precipitation simulated by 10 GCMs. *Climate Dyn.*, **19**, 383–395.
- Lau, K.-M., and S. Yang, 1996: Seasonal cycle, abrupt transition, and intraseasonal variability associated with the Asian summer monsoon in the GLA GCM. *J. Climate*, **9**, 965–985.
- , and —, 1997: Climatology and interannual variability of the Southeast Asian summer monsoon. *Adv. Atmos. Sci.*, **14**, 141–162.
- , K.-M. Kim, and S. Yang, 2000: Dynamical and boundary forcing characteristics of regional components of the Asian summer monsoon. *J. Climate*, **13**, 2461–2482.
- Lau, N.-C., M. J. Nath, and B. Wang, 2004: Simulations by a GFDL GCM of ENSO-related variability of the coupled atmosphere–ocean system in the East Asian monsoon region. *East Asian Monsoon*, C.-P. Chang, Ed., World Scientific, 271–300.
- Liang, J., S. Yang, C. Li, and X. Li, 2007: Long-term changes in the South China Sea summer monsoon revealed by station observations of the Xisha Islands. *J. Geophys. Res.*, **112**, D10104, doi:10.1029/2006JD007922.
- , —, Z.-Z. Hu, B. Huang, A. Kumar, and Z. Zhang, 2008: Predictable patterns of the Asian and Indo-Pacific summer precipitation in the NCEPCFS. *Climate Dyn.*, doi:10.1007/s00382-008-0420-8.
- Mahrt, L., and H.-L. Pan, 1984: A two-layer model of soil hydrology. *Bound.-Layer Meteorol.*, **29**, 1–20.
- Misra, V., and Y. Zhang, 2007: The fidelity of NCEP CFS seasonal hindcasts over Nordeste. *Mon. Wea. Rev.*, **135**, 618–627.
- Mitchell, K., R. Yang, J. Meng, and EMC Land Team, 2006: Initialization of the Noah Land Surface Model and its coupling to CFS. *31st Annual Climate Diagnostics and Prediction Workshop*, Boulder, CO, NOAA. [Available online at http://www.cpc.ncep.noaa.gov/products/outreach/proceedings/cdw31_proceedings/S3_03_Ken_Mitchell_NOAA_NCEP.ppt#259,2, Outline of Presentation.]
- Moorthi, S., H.-L. Pan, and P. Caplan, 2001: Changes to the 2001 NCEP operational MRF/AVN global analysis/forecast system. NWS Tech. Procedures Bull. 484, 14 pp. [Available online at <http://www.nws.noaa.gov/om/tpb/484.htm>.]
- Normand, C., 1953: Monsoon seasonal forecasting. *Quart. J. Roy. Meteor. Soc.*, **79**, 463–473.
- Pacanowski, R. C., and S. M. Griffies, 1998: MOM3.0 manual. NOAA/GFDL, Princeton, NJ.
- Peng, P., and A. Kumar, 2005: A large ensemble analysis of the influence of tropical SSTs on seasonal atmospheric variability. *J. Climate*, **18**, 1068–1085.
- Reynolds, R. W., N. A. Rayner, T. M. Smith, D. C. Stokes, and W. Wang, 2002: An improved in situ and satellite SST analysis for climate. *J. Climate*, **15**, 1609–1625.
- Saha, S., and Coauthors, 2006: The NCEP Climate Forecast System. *J. Climate*, **19**, 3483–3517.
- Sperber, K. R., 1994: Simulation of the northern summer monsoon in the ECMWF model—Sensitivity to horizontal resolution. *Mon. Wea. Rev.*, **122**, 2461–2481.
- , and Coauthors, 2001: Dynamical seasonal predictability of the Asian summer monsoon. *Mon. Wea. Rev.*, **129**, 2226–2248.
- Thiaw, W. M., and K.-C. Mo, 2005: Impact of sea surface temperature and soil moisture on seasonal rainfall prediction over the Sahel. *J. Climate*, **18**, 5330–5343.
- Wang, B., 2006: *The Asian Monsoon*. Praxis, 787 pp.
- , and Z. Fan, 1999: Choice of South Asian monsoon indices. *Bull. Amer. Meteor. Soc.*, **80**, 629–638.
- , R. Wu, and X. Fu, 2000: Pacific–East Asian teleconnection: How does ENSO affect East Asian climate? *J. Climate*, **13**, 1517–1536.
- , —, and T. Li, 2003: Atmosphere–warm ocean interaction and its impacts on Asian–Australian monsoon variation. *J. Climate*, **16**, 1195–1211.
- , I.-S. Kang, and J.-Y. Lee, 2004: Ensemble simulations of Asian–Australian monsoon variability by 11 AGCMs. *J. Climate*, **17**, 803–818.
- Wang, W., S. Saha, H.-L. Pan, S. Nadiga, and G. White, 2005: Simulation of ENSO in the new NCEP Coupled Forecast System Model. *Mon. Wea. Rev.*, **133**, 1574–1593.
- Webster, P. J., and S. Yang, 1992: Monsoon and ENSO: Selectively interactive systems. *Quart. J. Roy. Meteor. Soc.*, **118**, 877–926.
- , V. Magaña, T. Palmer, J. Shukla, R. Tomas, M. Yanai, and T. Yasunari, 1998: Monsoons: Processes, predictability, and the prospects for prediction. *J. Geophys. Res.*, **103**, 14 451–14 510.
- Wu, R., and B. P. Kirtman, 2004: The tropospheric biennial oscillation of the monsoon–ENSO system in an interactive ensemble coupled GCM. *J. Climate*, **17**, 1623–1640.

- Xie, P., and P. A. Arkin, 1996: Analyses of global monthly precipitation using gauge observations, satellite estimates, and numerical model predictions. *J. Climate*, **9**, 840–858.
- Yang, S., and K.-M. Lau, 2006: Interannual variability of the Asian monsoon. *The Asian Monsoon*, B. Wang, Ed., Praxis, 259–293.
- , P. J. Webster, and M. Dong, 1992: Longitudinal heating gradient: Another possible factor influencing the intensity of the Asian summer monsoon circulation. *Adv. Atmos. Sci.*, **9**, 397–410.
- , K.-M. Lau, S.-H. Yoo, J. L. Kinter, K. Miyakoda, and C.-H. Ho, 2004: Upstream subtropical signals preceding the Asian summer monsoon circulation. *J. Climate*, **17**, 4213–4229.
- , X. Ding, D. Zheng, and Q. Li, 2007a: Depiction of the variations of U.S. Great Plains precipitation and its relationship with tropical central-eastern Pacific SST. *J. Appl. Meteor. Climatol.*, **46**, 136–153.
- , —, —, and S.-H. Yoo, 2007b: Time-frequency characteristics of the relationships between tropical Indo-Pacific SSTs. *Adv. Atmos. Sci.*, **24**, 343–359.
- , M. Wen, and R. W. Higgins, 2008: Sub-seasonal features of the Asian summer monsoon in the NCEP Climate Forecast System. *Acta Oceanol. Sin.*, in press.
- Yoo, S.-H., C.-H. Ho, S. Yang, H.-J. Choi, and J.-G. Jhun, 2004: Influences of tropical western and extratropical Pacific SSTs on East and Southeast Asian climate in the summers of 1993–94. *J. Climate*, **17**, 2673–2687.
- , S. Yang, and C.-H. Ho, 2006: Variability of the Indian Ocean sea surface temperature and its impacts on Asian-Australian monsoon climate. *J. Geophys. Res.*, **111**, D03108, doi:10.1029/2005JD006001.
- Zhang, Q., and S. Yang, 2007: Seasonal phase-locking of the peak events in eastern Indian Ocean. *Adv. Atmos. Sci.*, **24**, 781–798.